Article

Ubiquitous GIS-Based Forest Fire Susceptibility Mapping Using Artificial Intelligence Methods

Seyed Vahid Razavi-Termeh [1,†] iD **, Abolghasem Sadeghi-Niaraki** [1,2,*,†] **and Soo-Mi Choi** [2] iD

[1] Geoinformation Tech. Center of Excellence, Faculty of Geodesy and Geomatics Engineering,
    K.N. Toosi University of Technology, Tehran 19697, Iran; vrazavi@mail.kntu.ac.ir
[2] Department of Computer Science and Engineering, Sejong University, Seoul 143-747, Korea;
    smchoi@sejong.ac.kr
* Correspondence: a.sadeghi@sejong.ac.kr
† These authors contributed equally to this work.

check for
updates

Abstract: This study aimed to prepare forest fire susceptibility mapping (FFSM) using a ubiquitous GIS and an ensemble of adaptive neuro fuzzy interface system (ANFIS) with genetic (GA) and simulated annealing (SA) algorithms (ANFIS-GA-SA) and an ensemble of radial basis function (RBF) with an imperialist competitive algorithm (ICA) (RBF-ICA) model in Chaharmahal and Bakhtiari Province, Iran. The forest fire areas were determined using MODIS satellite imagery and a field survey. The modeling and validation of the models were performed with 70% (183 locations) and 30% (79 locations) of forest fire locations (262 locations), respectively. In order to prepare the FFSM, 10 criteria were then used, namely altitude, rainfall, slope angle, temperature, slope aspect, wind effect, distance to roads, land use, distance to settlements and soil type. After the FFSM was prepared, the maps were designed and implemented for web GIS and mobile application. A receiver operating characteristic (ROC)- area under the curve (AUC) index was used to validate the prepared maps. The ROC-AUC results showed an accuracy of 0.903 for the ANFIS-GA-SA model and an accuracy of 0.878 for the RBF-ICA model. The results of the spatial autocorrelation showed that the occurrence of fire in the study area has a cluster distribution and most of the spatial dependence is related to the distance to settlement, soil and rainfall variables.

Keywords: forest fire; artificial intelligence; ubiquitous GIS; ensemble models; mobile application

1. Introduction

Forests are among the most important natural resources that have positive ecological, economic and social effects [1]. In recent years, due to population growth and industry development, the use of natural resources, especially forests, to supply food and materials has been increasing [2]. Different human and natural factors can lead to forest fires [3]. Changing and transforming ecosystems to increase agricultural land use/cover by farmers and foresters [4] is one of the global issues that annually destroys 16 million hectares of the world's forested area [5]. After agricultural and urban activities (air pollution, noise pollution, groundwater pollution and land degradation), a forest fire is the second factor for ecosystem degradation [3]. According to the organization of forests in Iran, forest fires occur repetitively in Iran, which reduces 5000 to 6000 hectares of forest area annually [5]. Iran is located in the desert high-pressure subtropical zone on the Earth, which provides the proper conditions for forest fires [6]. The factors that increase forest fires in Iran include tourist imprudence by lighting camp fires in forests, deliberate fires to convert forests into agricultural lands [6,7], firelight, drought season and hot winds [5,8]. Due to the destruction of rangelands and forests in different parts of Iran, it is necessary to prepare a fire hazard map and identify vulnerable areas in order to predict and prepare in advance

to address the issue especially in the Zagros mountains. Until now, many models have been utilized to prepare the forest fire susceptibility mapping (FFSM) based on GIS and remote sensing (RS) [9–11]. The GIS-based approaches that are used to prepare FFSMs include statistical methods, such as frequency ratio (FR) [12], evidential belief function (EBF) [13], weight of evidence (WOE) [14], machine learning and data mining (random forest (RF) [15], gradient boosted decision trees [16], ensemble adaptive neuro fuzzy interface system (ANFIS) with particle swarm optimization [17], boosted regression trees (BRT) [18], linear and quadratic discriminant analyses (LDA-QDA) [12], support vector machines (SVM) [15], logistic regression (LR) [10], artificial neural networks (ANN) [19], and multi-criteria decision-making [20]. The result of a traditional GIS analysis is displayed in two-dimension on the map, but users who are not familiar with spatial knowledge or spatial information have difficulty understanding and analyzing the results [21]. Spatial information has evolved from paper-based GIS maps to web-based GIS over time, and it has finally evolved to become the current ubiquitous GIS [22,23]. The ubiquitous GIS provides services to any user anytime and anywhere using sensors. The user interactivity with the environment is enhanced using information technology and mobile infrastructure, such as sensor networks and the internet [24]. To date, little research has been done on forest fires using mobile GIS, web GIS and ubiquitous GIS technologies. In this regard, Dong et al. [25] used a GIS mobile system to manage forest information. Battad and Mackenzie [26] used a mobile GIS system to manage the forest in southern Australia. Kalabokidis et al. [27] used a web GIS system to control forest fires and generate virtual fire. Barbosa et al. [28] provided a forest fire alert system using a web GIS model for the Amazon forest in Brazil. Jeefoo [29] used a mobile GIS system to determine forest fire points in the Nan province, Thailand. The innovation of the present study was to provide an FFSM using artificial intelligence methods under a ubiquitous GIS system on a mobile GIS system. Therefore, the purpose of this research was to prepare an FFSM based on ubiquitous GIS using the ensemble ANFIS with combined genetic (GA) and simulated annealing (SA) algorithms as well as combining the radial basis function (RBF) interpolation method imperialist competitive algorithm (ICA) algorithm. Hitherto, Jaafari et al. [2,24] used the combined ANFIS method with GA, the firefly algorithm (FA), particle swarm optimization (PSO), the shuffled frog leaping algorithm (SFLA) and an ICA algorithm to produce an FFSM in Chaharmahal and Bakhtiari province, Iran. Moayedi et al. [30] optimized the ANFIS model using GA, PSO, and differential evolution (DE) algorithms to prepare an FFSM in a region of Iran. According to the results, the ANFIS-GA model has a higher accuracy than other models in preparing forest fire maps. Hong et al. [31] used a GA algorithm to determine the optimal parameters affecting forest fires and then prepared an FFSM using the RF and SVM models in the southwest of Jiangxi Province, China. Zhang et al. [32], using the convolutional neural network model, prepared an FFSM in the Yunnan Province of China. Bui [33] optimized the ANN model using biogeography-based optimization, the gravitational search algorithm, and grey wolf optimization to prepare an FFSM in Dak Nong, Vietnam. Thus far no research has used a combination of the two metaheuristic algorithms with ANFIS to prepare an FFSM. The innovation of the present study was to combine the two metaheuristic algorithms with ANFIS, optimize the RBF with the ICA algorithm, and present an FFSM in the ubiquitous system as a mobile application.

2. Materials and Methods

2.1. Study Area

The study area was located in the western Zagros Mountain in Chaharmahal and Bakhtiari province, Iran. The coordinates of this region area ware between latitudes of 32′6° N to 32′43° N and longitudes of 50′20° E to 51′11° E. The size of the study area was approximately 2933 km^2 and consisted mainly of an elevated mountainous region. The minimum and maximum altitude in the region were 1800 and 3304 m. The region has a temperate semi-humid climate with mild summers and severe winters. The average annual temperature is 11.5 °C. January is the coldest month of the year and August is the hottest. Most of this area is forested with Oak, Quercus persica, Olea europaea L,

Pistacia khinjuck, Crataegus aronia and Prunus dulcis. Most fires occur during the dry season from July to August. The study area along with the fire locations are shown in Figure 1.
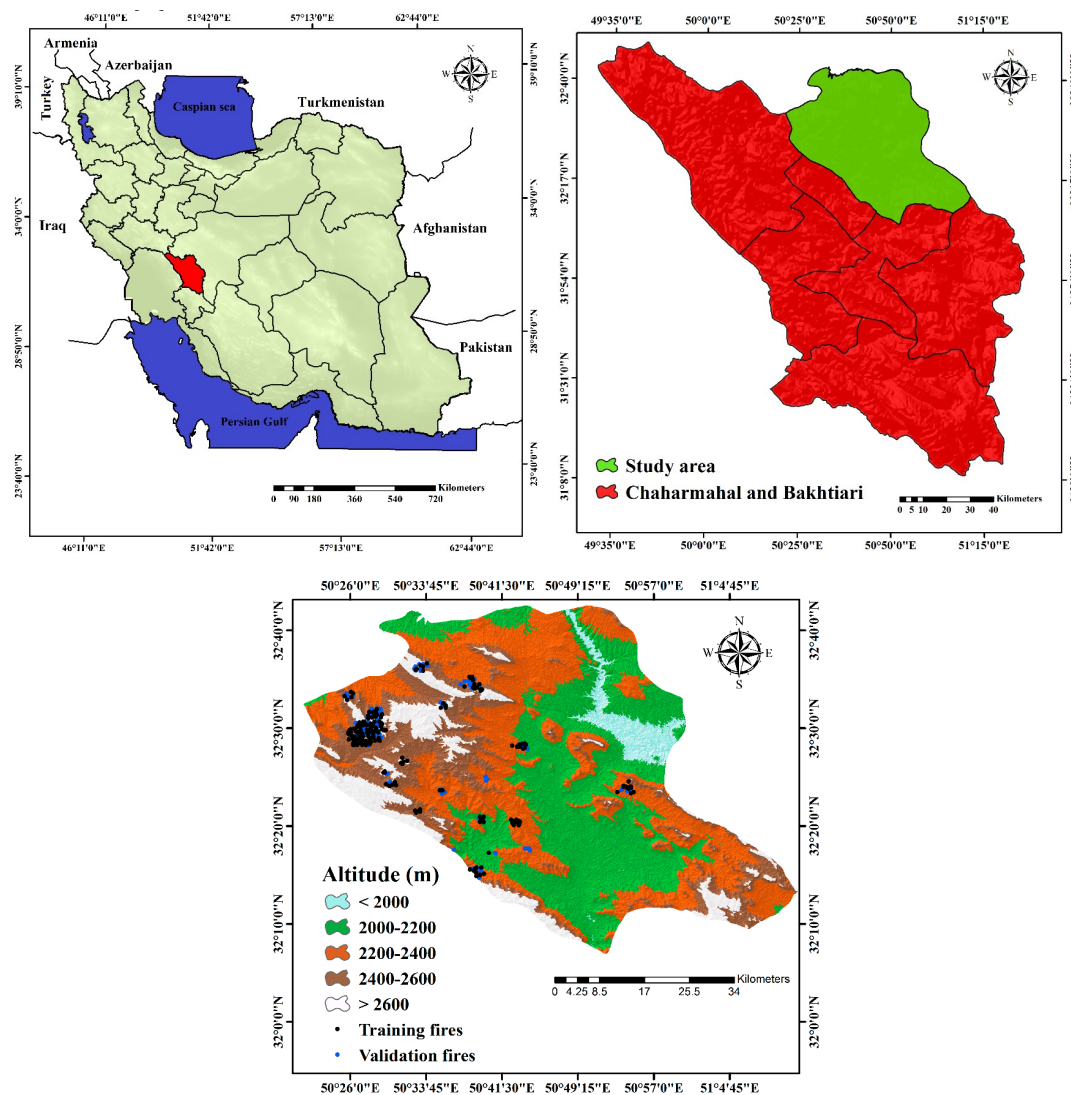

Figure 1. Study area with the fire locations.

2.2. Methods

2.2.1. FR Model

One of the statistical bivariate models is FR, which is widely used in modeling environmental hazards such as floods, landslides and forest fires. The model assumes that a future hazard will occur in places with similar conditions and characteristics of the past hazards [34]. For FR estimation, the ratio of fire zones to the entire study area was calculated (Equation (1)):

$$FR = \frac{\frac{Npix\ (SX_i)}{\sum_{i=1}^{m} SX_i}}{\frac{Npix\ (X_j)}{\sum_{j=1}^{n} Npix\ (X_j)}} \tag{1}$$

In Equation (1), $Npix\ (SX_i)$ is the number of fire pixels in the ith class of variable x. $Npix\ (X_j)$ is the total number of variable pixels X_j, and m and n are the number of categories and the total number of criteria, respectively.

2.2.2. ANFIS Model

ANFIS is a hybrid system that combines the ability of fuzzy logic decision making with neural network computation capability and offers a high level of sophisticated modeling and estimation [35]. This system has the advantage of both models in the sense that it utilizes the neural network training features and the high decision-making power of the fuzzy systems in certain and uncertain conditions. The model uses an error propagation algorithm and a hybrid to train the network, reduce the algorithm's complexity and enhance the network learning. In addition, the fuzzy inference system utilized was the Sugeno model, which was used to derive the fuzzy rules and outputs of the system [36].

2.2.3. GA Algorithm

The GA algorithm is based on the theory of evolution and it is among the first and most famous metaheuristic algorithms [37]. The basis of the GA is to convert each set of answers into a binary encoder called a chromosome. Each chromosome in the GA represents a search space point and a possible solution to the problem. The implementation of the algorithm starts with the creation of an original set of random alternatives called the original population [38]. Each algorithm iteration generates a new set of chromosomes called generations. The quantity of chromosomes is determined by the fitness function throughout each generation. During the reproduction process, genetic operators, which include fusion and mutation, are applied to the chromosomes. The fitness function evaluates each chromosome, and the genetic operator selects it. Finally, the best chromosomes are selected and transferred to the next generation that represents the optimal solution to the problem [39].

2.2.4. SA Algorithm

The SA algorithm is an optimization algorithm that is easy and efficient to use for solving optimization issues. It originates from the work of Patrick and Kearney and their colleagues in 1983 [40]. They proposed a method based on a gradual simulated technique to solve complex optimization problems [41]. The SA algorithm begins with an original solution and moves in an iteration loop to the adjacent solution. If the neighbor's answer is better than the original answer, the algorithm sets it as the original answer and if it is not better the algorithm accepts the original answer with the likelihood [42]. Several repetitions are performed at each temperature while the temperature gradually decreases. The initial steps set the temperature in order to accept worse responses. With the gradual decreasing of the temperature, the final steps are less likely to accept worse solutions, which converges the algorithm to a good solution [41].

2.2.5. ICA Algorithm

The ICA algorithm is based on the evolution of human society and politics [43]. It begins with a random number of populations, and each one is called a state. The best ones are chosen as imperialists (colonists) in the population and the remainder are regarded as colonies [44]. Depending on their power, the colonists draw the colonies as described subsequently. The empire's strength relies on its two constituent components, which include the imperialist state and its colonies. This dependence is based mathematically on the definition of imperial strength as the sum of the power of the imperialist plus the average power of its colonies. The imperialist competition between them starts with the formation of the early empires. Any empire that fails to enhance its strength will be removed from the colonial competition. Hence, an empire's survival will depend on its ability to dominate the rival empire colonies. The strength of larger empires is enhanced during the colonial competition, and the weaker empires disappear. Over time, the colonies will get closer to the empires to form a kind of convergence as far as power is concerned. The final phase of the colonial competition is to build a single universal empire in the globe that is much closer to the empire with colonial nations [43].

2.2.6. RBF Model

The RBF interpolation model is a spline interpolation method used when the modeling process is time consuming. Unlike neural network-based prediction methods, this model provides a function estimation with much a lower computation and a higher accuracy [45]. This model estimates new values in a new position of samples by applying the base points. For this purpose, the method computes an interpolation function based on the sum of the observed data as in Equation (2) [45]:

$$\eta(x) = \sum_{j=1}^{m} p_i \varphi\left(\|x - x^j\|\right) \tag{2}$$

where $\|x - x^j\|$ represents the Euclidean distance of two points, p is the weighting factor and φ is the radial basis function.

3. Research Framework

In this paper, the FFSM was developed in seven main stages. The property of the region was defined in the first step and the fires that occurred were recognized. The data were gathered in the second stage, and an efficient spatial database was structured with forest fire conditioning variables. In the third stage, the spatial connection between the forest fire effective factors and the inventory map of the fires were employed in an FR model. The ANFIS-GA-SA and RBF-ICA models were implemented using the weights obtained from the FR in the fourth step. In the fifth step, the FFSM was prepared employing the ANFIS-GA-SA and RBF-ICA models. In the sixth step, the mobile application (UFFSM) was designed and implemented in a ubiquitous GIS system. In the last step, a ROC curve validated the FFSM. A summary of the research steps is shown in Figure 2.
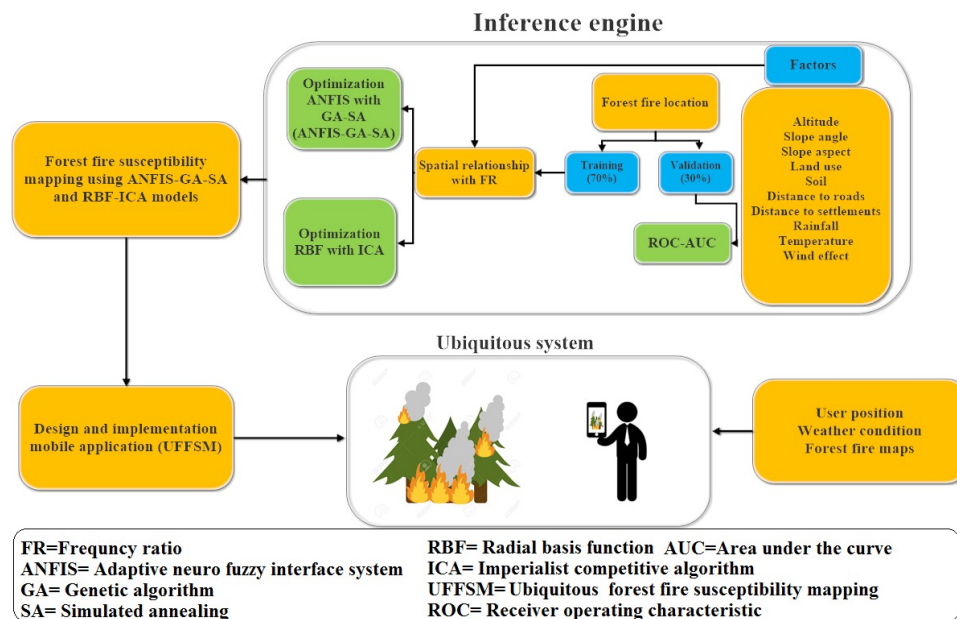

Figure 2. Methodology flowchart.

3.1. Spatial Database

3.1.1. Forest Fire Inventory

Previous fire data were obtained from the Chaharmahal and Bakhtiari natural resource bureau, MODIS hot spot products (http://earthdata.nasa.gov/firms) satellite imagery, and surveying data from 2013 to 2018. A total of 262 fire hotspots were identified in the study area with a 1 km buffer. Taking into

account the 70:30 ratio, dividing the data into two sections of training and validation data randomly, 183 locations of the fires (70%) were used to build the model and 79 locations (30%) were considered to validate the models (Figure 1).

3.1.2. Criteria Affecting Forest Fire

Topographic factors: Altitude, slope angle and slope aspect WEre topographical variables influencing the occurrence of fires. Topographic features and the direction of the wind also affect the likelihood of fires in the area [46]. The study area's digital elevation model (DEM) was prepared with a spatial resolution of 30 m from the ASTER satellite images. Then, the map of altitude, slope angle and slope aspect were extracted from the ArcGIS10.3 software. Altitude changes can influence the temperature and vegetation: since higher altitude areas have a lower temperature and a higher humidity, the likelihood of a fire is inversely correlated with a higher altitude [47] (Figure 3a). The slope angle affects the direction and extent of the fire. Generally, the degree of damage is higher in steeper slopes [48] (Figure 3b). The slope aspect is affected by the quantity of sunlight and heat associated with the area's plant dryness [49]. In general, the south and east directions have the highest rate of sunlight exposure and are more prone to fires [49] (Figure 3c).

Socio-economic factors: With increasing population in recent decades, the invasion of the forest areas to obtain supplies, fuel and agriculture has been frustrating. The residents of the surrounding forest areas are dependent on the forest [2]. The role of tourists in creating fires is also undeniable. Therefore, three factors, namely the distance to roads, land use and the distance to settlements were used as socio-economic factors in this study. In general, there is a greater likelihood of a fire near the road [18]. For this purpose, the road maps of the study area were prepared using 1: 100,000 topographic maps and buffers for the roads were defined at specified intervals (Figure 3f). Other influencing factors that affect forest fires are the proximity to a settlement (rural and nomadic settlements). As residents are dependent on the forest and land to provide for their needs, they may set deliberate and unintentional fires [50]. The distance from a settlement map was prepared using 1: 100,000 topographic maps (Figure 3g). Landsat-7 images from 2013 and 2018 were used to prepare the land use/cover map. For this purpose, 400 training points collected with the Global Positioning System (GPS) were used to build the land use/cover map, of which 70% of these data were used for training and the remaining 30% were used to evaluate the accuracy of the map. The land use/cover maps using the maximum likelihood algorithm at an accuracy of 91% were obtained and split into five classifications: forests, agricultural, pastures, wilderness and urban areas (Figure 3d).
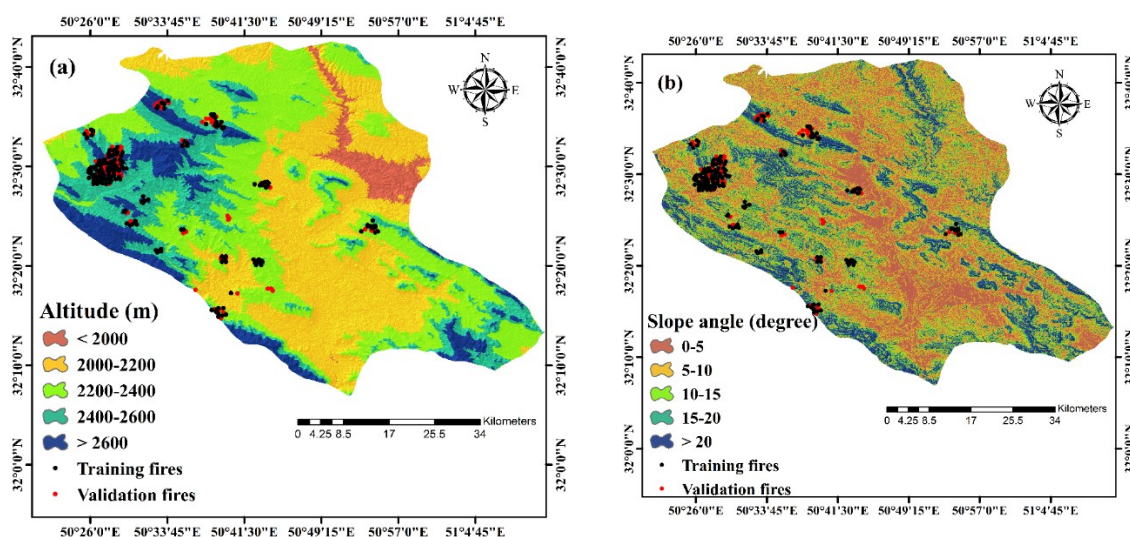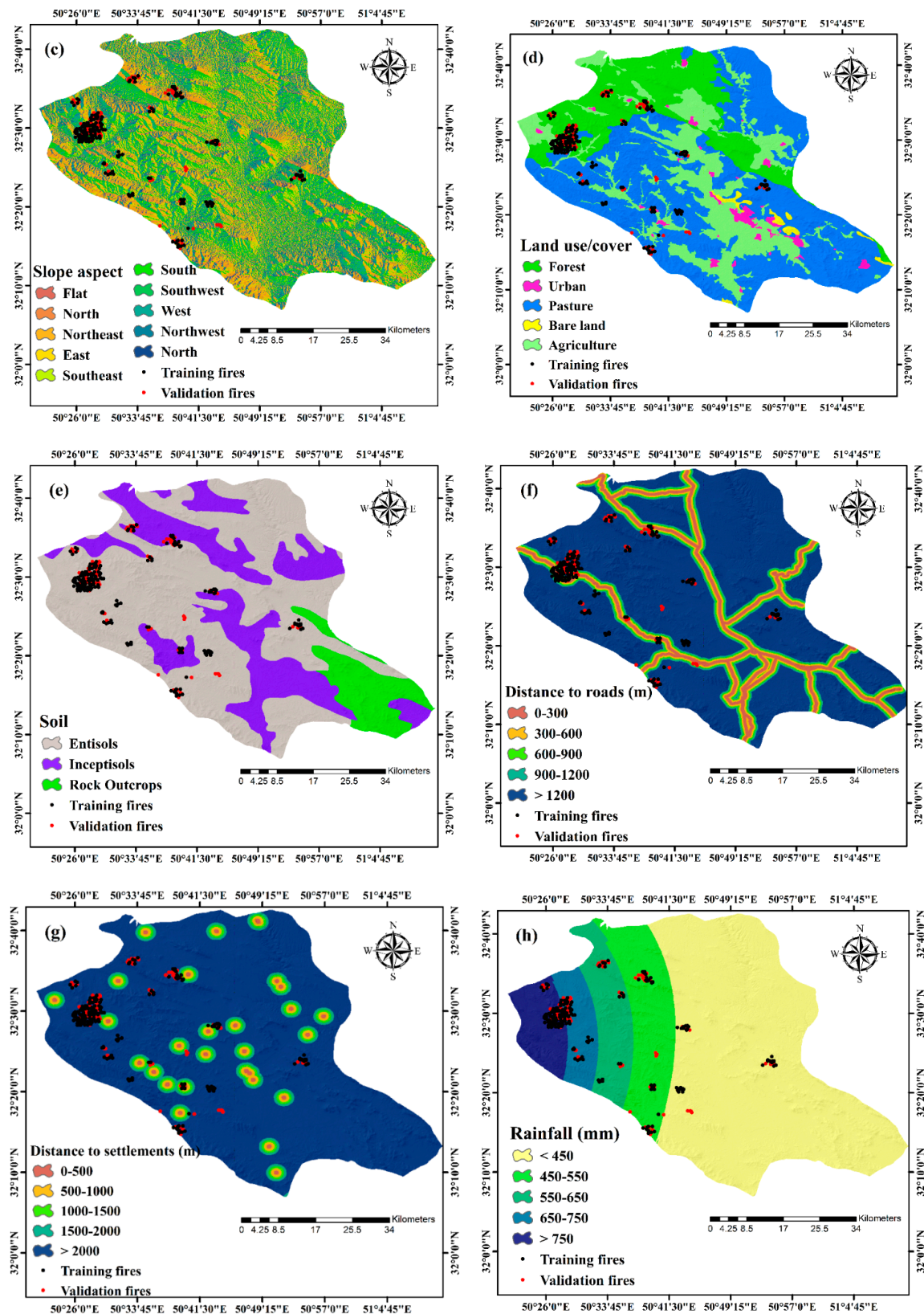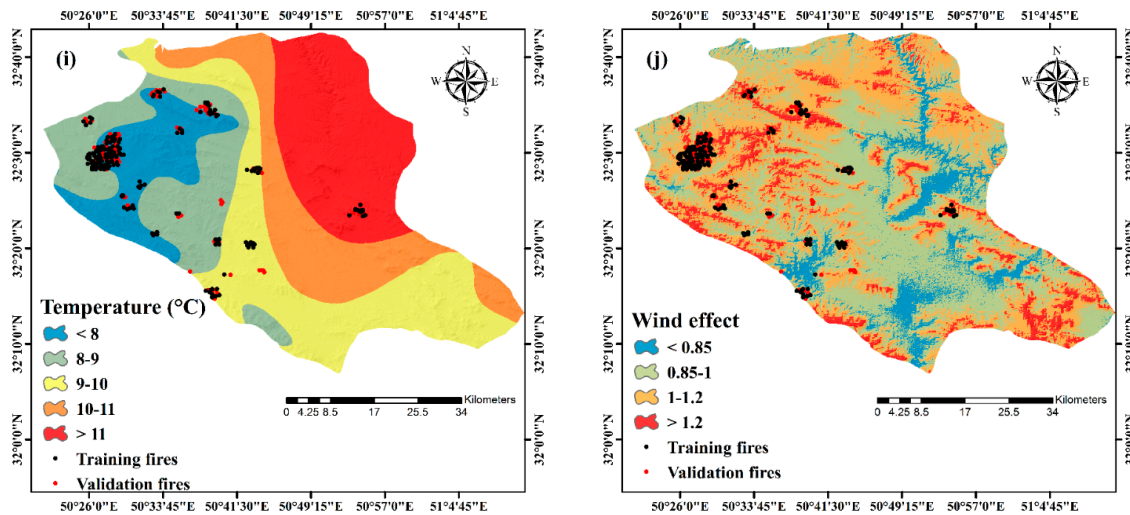

Figure 3. *Cont.*

Figure 3. *Cont*.

Figure 3. Forest fire effective criterion: (**a**) the altitude; (**b**) the slope angle; (**c**) the slope aspect; (**d**) the land use/cover; (**e**) the soil; (**f**) the distance to roads; (**g**) the distance to settlements; (**h**) the rainfall; (**i**) the temperature and (**j**) the wind effect.

Climatic factors: Climatic conditions affect forest fires directly and indirectly, and they affect the vegetation type and density indirectly [48]. In this study, the mean annual data for rainfall, temperature, speed and direction were obtained from 14 meteorology stations in Chaharmahal and Bakhtiari province from 2013-2018. The Kriging interpolation method was used to prepare the rainfall and temperature maps. Windward and Leeward indexes in the system for automated geoscientific analyses (SAGA)-GIS software were used to construct the wind effect map. The input of these indexes were the DEM, speed and the direction of the wind. In general, areas with higher temperatures and lower rainfall affect the occurrence of fires [2] (Figure 3h–j).

3.2. Analysis of Forest Fire Hotspot

3.2.1. Analysis of Fire Frequency and Fire Cycle

In this study, fire frequency and fire cycle indicators were used to analyze the forest fire locations. Fire frequency is the number of times fires occur within a given region and period [51]. Fire cycle is the time required for the burning of an area equal to a given landscape area. During this phase, the whole area may not burn; some places may burn several times and others may not burn at all [52]. The fire cycle was calculated using Equation (3):

$$Fire\ cycle = \frac{T_a \times T_y}{T_b} \tag{3}$$

where T_a is the total study area, T_y is the number of years and T_b is the total area *Fire cycle* = burned.

3.2.2. Spatial Autocorrelation Analysis

Semivariogram

The semivariogram chart is based on the distance between the samples, which indicates the spatial relationship between the samples [53]. The semivariogram was calculated using Equation (4):

$$\gamma(h) = \frac{1}{2N(h)} \sum_{i=1}^{N(h)} [Z(x_i) - Z(x_i + h)]^2 \tag{4}$$

where $\gamma(h)$ is the value of the semivariogram for n pairs of samples separated by a distance of h. $Z(x_i)$ and $Z(x_i + h)$ are also x local variables at points i and i+h.

The three components of range, sill and nugget are used to describe and model the semivariogram. The range is called the distance at which the variogram reaches a fixed point and approaches the horizontal line. This range specifies the range in which the data can be used to estimate the value of the unknown variable, and outside of this distance, there is no more spatial continuity, and the samples operate independently [52]. The sill parameter is the constant value that the variogram reaches in the range parameter. This is equal to the variance of the total number of samples used to calculate the variogram. The amount of the variogram at the origin of the coordinates (h = 0) is called the nugget that shows the variable structure except randomly and ideally should be zero [54]. The spatial dependence (SD) was calculated using the nugget and partial sill parameters according to Equation (5):

$$SD = \frac{nugget}{nugget + partial\ sill} \times 100 \tag{5}$$

If the SD rate is less than 25%, the variable has a strong spatial dependence, if the rate is between 25% and 75%, the variable has a moderate spatial dependence, and if the rate is more than 75%, the variable has a weak spatial dependence [55].

Moran's I Index

The Moran's I index includes the general and local Moran's I indicators, which are considered as essential tools in examining the spatial relationship of data with each other [56]. The range of values of the general Moran's I index indicator can vary from −1 to +1. The amount of +1 indicates the highest degree of positive spatial correlation, the amount of −1 indicates the highest degree of negative spatial correlation and zero shows the maximum degree of the random distribution of values [57]. The general Moran's I index indicator shows the presence or absence of a general spatial correlation in the data. The local Moran's I index indicator can indicate the degree of spatial correlation of the variable at any point [58]. The general Moran's I and local Moran's I indicators can be calculated using Equations (6) and (7):

$$I = \frac{n}{\sum_{i=1}^{n} \sum_{j=1}^{n} w_{ij}} \times \frac{\sum_{i=1}^{n} \sum_{j=1}^{n} (z_i - z)(z_j - z) w_{ij}}{\sum_{i=1}^{n} (z_i - z)^2} \tag{6}$$

$$I_i = \frac{x_i - \overline{X}}{\frac{\sum_{j=1.j\neq1}^{n} w_{ij}}{n-1} - \overline{X}^2} \sum_{j=1.j\neq i}^{n} w_{ij}(x_i - \overline{X}) \tag{7}$$

In the above equations, Z is the average value of the variable z, z_i is the value of the variable in location of i, z_j is the value of the variable in location of j, $\overline{X}$ is the mean of the descriptive values, x_i is the value of the location I, w_{ij} is the spatial co-weight between i and j and n is the total number of complications.

3.3. Combining ANFIS with Hybrid Algorithm

To date, ANFIS has been utilized with a descending gradient and the least-square techniques. The least square methods are effective to optimize parameters, and the preceding parameters are of great importance in modeling [59]. These methods were not appropriate due to their high complexity with gradient calculations and the nonlinear presence of preceding parameters in the output [60]. Therefore, metaheuristic algorithms were used to train the ANFIS to solve this problem. Each metaheuristic algorithm has some advantages and disadvantages. A GA algorithm was combined with a SA algorithm to improve the network training accuracy.

The proposed algorithm initially functioned as a GA algorithm. If the best chromosome found during the last five generations does not change or the GA algorithm is repeated 10 times, which is half the termination condition for the GA algorithm, then the SA algorithm becomes active. The best

solution for the GA algorithm is selected as the first solution for the SA algorithm for this purpose, and it then performs the rest of the calculations [61]. The proposed algorithm works as follows:

Step 1—An original chromosome population is chosen;

Step 2—The current generation is increased by using mutation and integration operators;

Step 3—If the best chromosomes are not found in five consecutive iterations or the iteration has been repeated more than 10 times, which is half the termination condition, then the best current chromosome is considered as the input for the SA algorithm;

Step 4—The current solution is improved using the SA algorithm;

The objective function to train the ANFIS in the combined algorithm is shown in Equations (8) and (9). The purpose is to minimize the RMSE value [62]:

$$RMSE = \sqrt{Mean\left((t - y)^2\right)} \tag{8}$$

$$\text{Objective function} = \min (RMSE) \tag{9}$$

where t and y are the target data and input data, respectively.

3.4. Combining RBF Interpolation Method with ICA Algorithm

Each class's weight is assigned to the rest of the class in bivariate statistical techniques, such as FR. In natural hazards, the features are not in a crisp state. Therefore, the weight assigned to the whole class cannot be a satisfactory solution [63]. In the first step, the factors affecting forest fires were determined and each factor was classified according to the experts' opinion. In the second step, the weights of each class were determined using an FR model. In this study, the conditioning factors were divided into two categories that were the continuous and discrete data. The continuous factors consisted of the slope angle, altitude, slope aspect, temperature, wind effect, rainfall, distance to roads and the distance to settlements. The discrete factors included soil and land use.

First, the weight of each category was assigned to the middle of that category for the continuous factors [63]. Then, the weights for all the values of that factor were calculated using the ensemble model. For the discrete data, the weighted layers from the FR model were used to produce the final FFSM. For this purpose, the center of each class of factor was considered as training data in the RBF interpolation method, and the RBF fit the best function according to the training data. For optimizing and training the RBF method, the colonial competition algorithm was used. The objective function of the combined algorithm is shown in Equation (10):

$$object\ function = \sum_{i=1}^{n} w_i \times exp\left(-\frac{1}{2}\left(\frac{x - m_i}{\sigma_i}\right)^2\right) \tag{10}$$

where m, σ and w are the middle of the kernel function and the deviation and coefficients of weight, respectively.

3.5. Ubiquitous GIS

Mark Weiser first introduced the term ubiquitous computing in 1988 [64]. According to this theory, future computer technologies will progress in such a way as to be accessible in human lives to help them with their daily activities [65]. Ubiquitous computing platforms have created an intelligent environment using transparent interaction, automated capture, knowledge of the environment, context awareness, the automatic activation of systems and proactive and reactive commands by the users [66]. Ubiquitous GIS offers new systems utilizing interdisciplinary computing in spatial information-related issues and applications [67]. In the ubiquitous GIS context, every service was provided to every user at any place, at any time, by any means and under any network. In other words, ubiquitous GIS is the fourth generation of spatial information system created by adding knowledge and simplicity to the spatial information and internet [23,68].

3.6. Validation and Comparison

The model's efficiency was assessed using a ROC curve and AUC. For each probability value, the ROC technique was the graphical depiction of the balance between the false positive and the false negative [62]. The AUC is the prediction of the model by describing its ability to estimate an event accurately. The AUC varies from zero to one. Overall, an AUC between 0.8-1 indicates a very good performance, 0.7–0.8 indicates a good performance, 0.6–0.7 indicates a moderate performance, and 0.5–0.6 indicates a poor model performance [69].

The distinction between the observed and the estimated values of the models is produced by prediction error, which is used to assess the precision of the models [62]. Root mean square error (RMSE) is the difference between the value predicted by the model and the actual value and mean absolute error (MAE) is a measure of errors between paired observations [62]. The RMSE and the MAE indexes were used in this research to assess the efficiency and predictive precision of the suggested model. (Equations (11) and (12)):

$$\text{RMSE} = \sqrt{\frac{\sum_{i=1}^{n}(y_i - \hat{y}_i)^2}{n}} \tag{11}$$

$$\text{MAE} = \frac{\sum_{i=1}^{n}|y_i - \hat{y}_i|}{n} \tag{12}$$

where n is the sum of the total data, y_i is the observed values and $\hat{y}_i$ is the predicted values.

4. Results

4.1. Results of Forest Fire Hot Spot Analysis

The results of the fire frequency from 2013 to 2018 are shown in Figure 4. According to the results, the highest quantity of fires was related to 2018 with 56 cases, and the lowest quantity of fires related to 2014 was 28 cases. The results show that the frequency of the fires in the study area was ascending and the burned areas also increased.
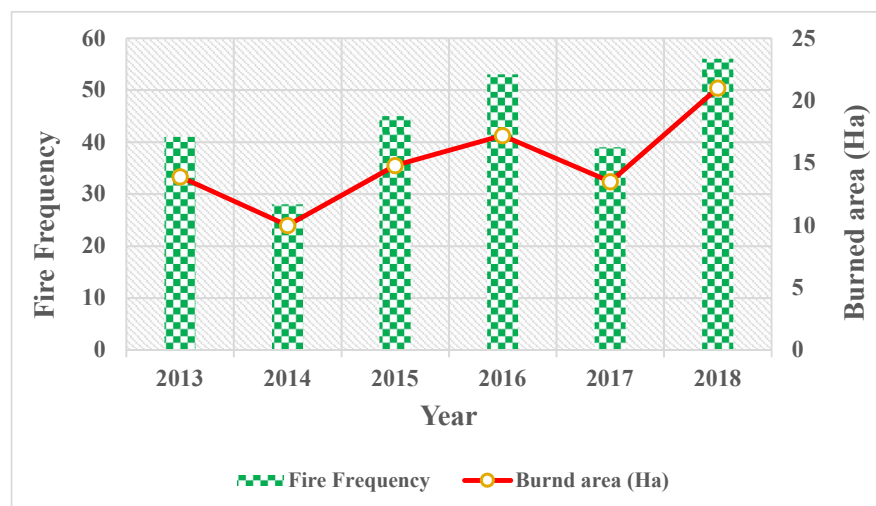

Figure 4. Result of the fire frequency.

The results of the fire cycle are shown in Figure 5. The lowest value of this index was related to 2018, 2016 and 2015, respectively. A lower value of this indicator indicates a higher probability of forest fire. According to the results of the fire frequency and the fire cycle, the probability of a fire from 2013 to 2018 was increasing.
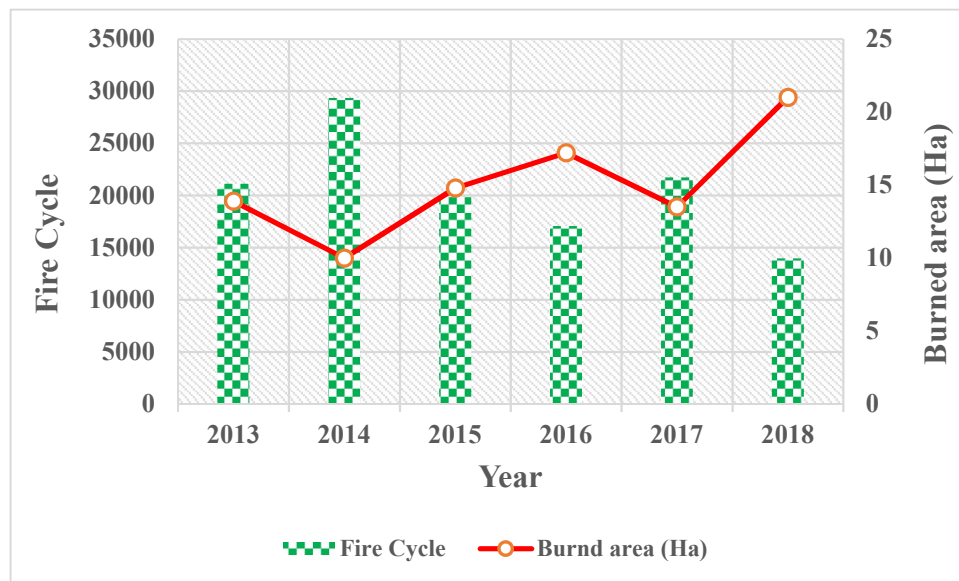
Figure 5. Result of the fire cycle.

4.2. Results of Spatial Autocorrelation

In the analysis of spatial correlation, the parameters of the number of years of fire occurrence and fire radiative power (FRP) were used. The results of the semivariogram parameters are shown in Table 1 and Figure 6. According to the results, the value of the nugget parameter of the fire year was less than the FRP, while the two parameters of range and partial sill on FRP were higher than the fire year. According to the SD index results, the year has a strong spatial dependence than FRP. Therefore, in preparing the forest fire probability map, using the data of the fire year can have better results than the FRP.
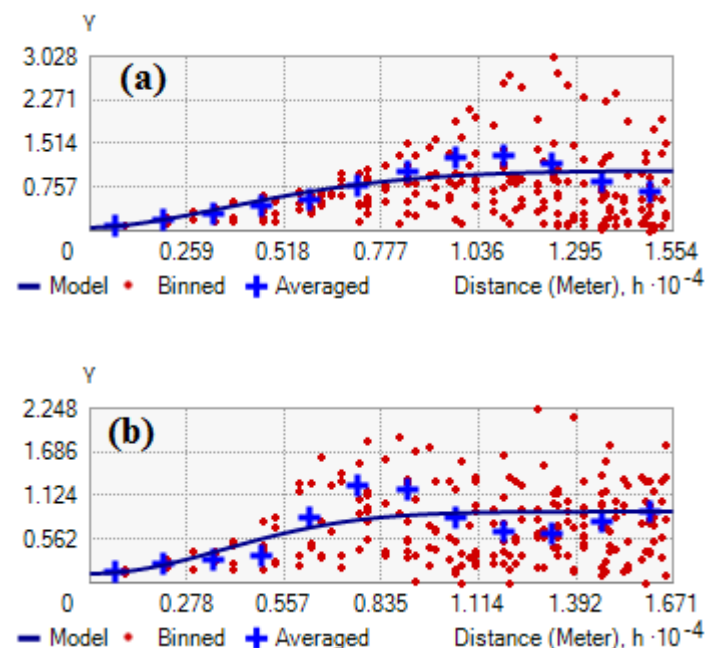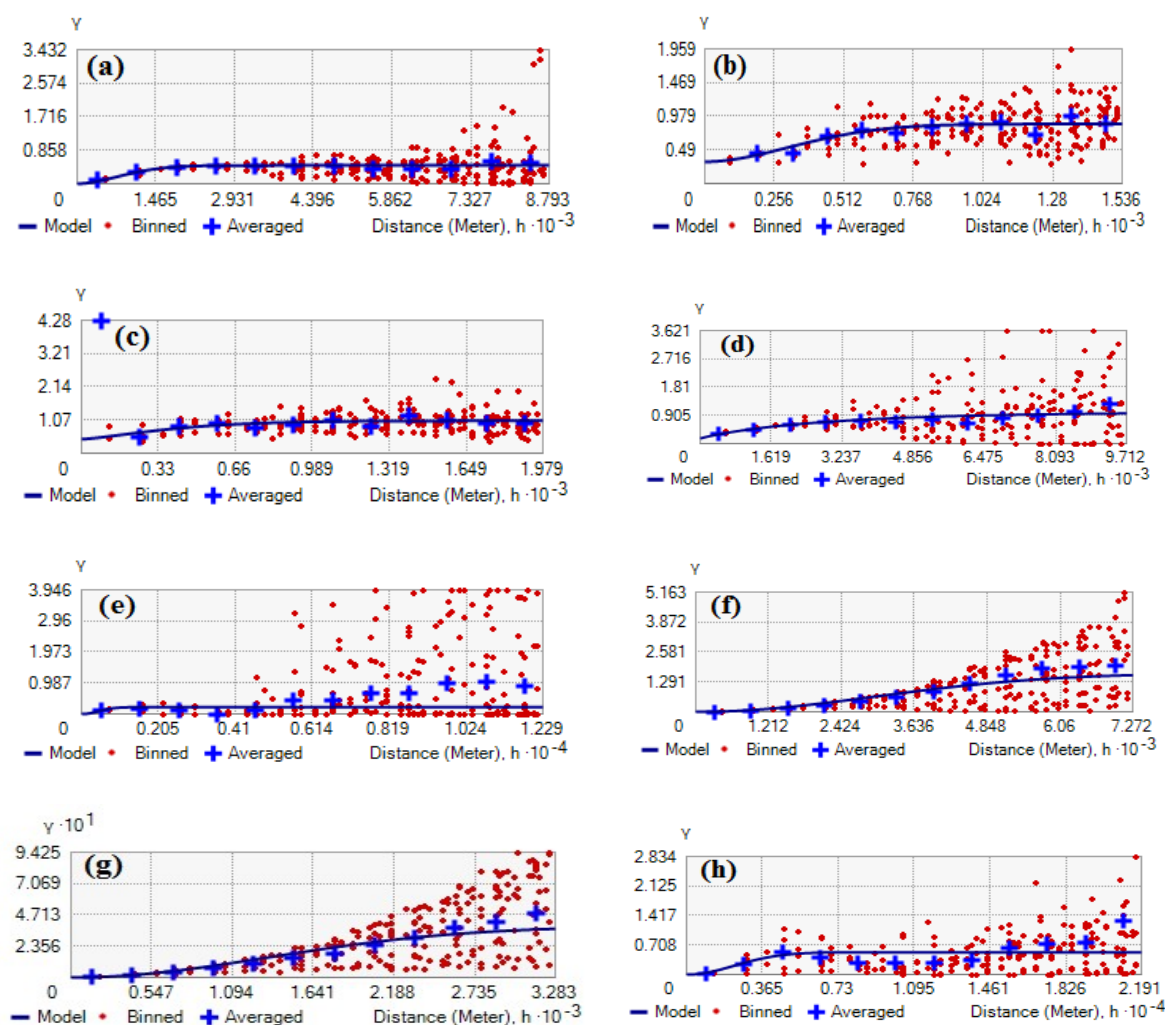

Figure 6. Result of the spatial autocorrelation of (**a**) the forest fire years and (**b**) the fire radiative power (FRP).

Table 1. Result of the semivariogram parameters.

Parameters	Year	FRP
Nugget	0.05905	0.12032
Range	11,128.985	9379.807
Partial sill	0.98964	0.79757
SD	5.63%	13.1%

The results of the semivariogram of the variables are shown in Figure 7 and Table 2. Based on the results, the soil, rainfall and distance to settlements variables had the lowest value of the nugget parameter, and the slope aspect, slope angle and the wind effect variables had the highest value of this parameter. In the range parameter, the highest value was related to temperature, land use/cover and the distance to roads variables, and the lowest value was related to the soil, slope aspect and the slope angle variables. The results of the sill parameter showed that the highest value of this parameter was related to the variables of distance to roads, temperature and the land use/cover and the lowest value was related to the altitude, soil and the distance to settlements variables. According to the results of the SD index, the highest value was related to the distance to settlements, soil and the rainfall variables, and the lowest value of this parameter was related to the wind effect, slope angle and the slope aspect variables.
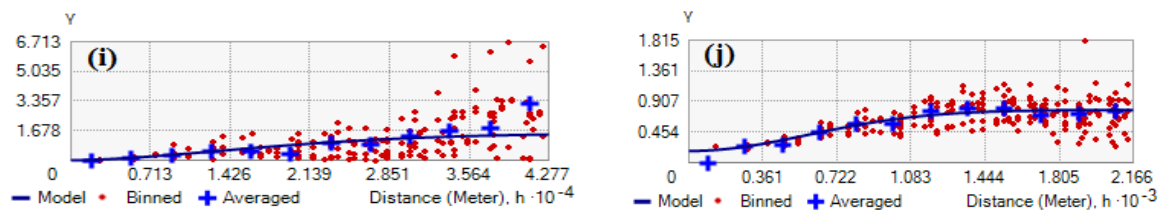

Figure 7. *Cont.*

Figure 7. Spatial autocorrelation results by the related factors: (**a**) the altitude; (**b**) the slope angle; (**c**) the slope aspect; (**d**) the land use/cover; (**e**) the soil; (**f**) the distance to roads; (**g**) the distance to settlements; (**h**) the rainfall; (**i**) the temperature; and the (**j**) wind effect.

Table 2. Results of the semivariogram parameters by the related factors.

Criterion	Nugget	Range	Partial Sill	SD
Altitude	0.004922	2024.1648	0.46849	1.039%
Soil	0.000219	1062.7202	0.21937	0.09973%
Aspect	0.4578	1016.6755	0.59021	43.68%
Land use/cover	0.16668	9711.9053	0.84549	16.46%
Wind effect	0.17483	1419.19543	0.60667	22.37%
Distance to settlements	0.00107	3282.508	0.38529	0.027%
Temperature	0.00863	42770.0009	1.5347	0.56%
Slope	0.31877	809.9563	0.549258	36.72%
Rainfall	0.000536	5560.5048	0.5366	0.09978%
Distance to roads	0.0016685	7272.40635	1.668506	0.0998%

The results of the Moran's I index are shown in Figure 8 and Table 3. According to the results, the value of Moran's I index for the parameters of year and FRP was 0.830061 and 0.904367, respectively. According to the results, the year and FRP variables had the cluster distribution.
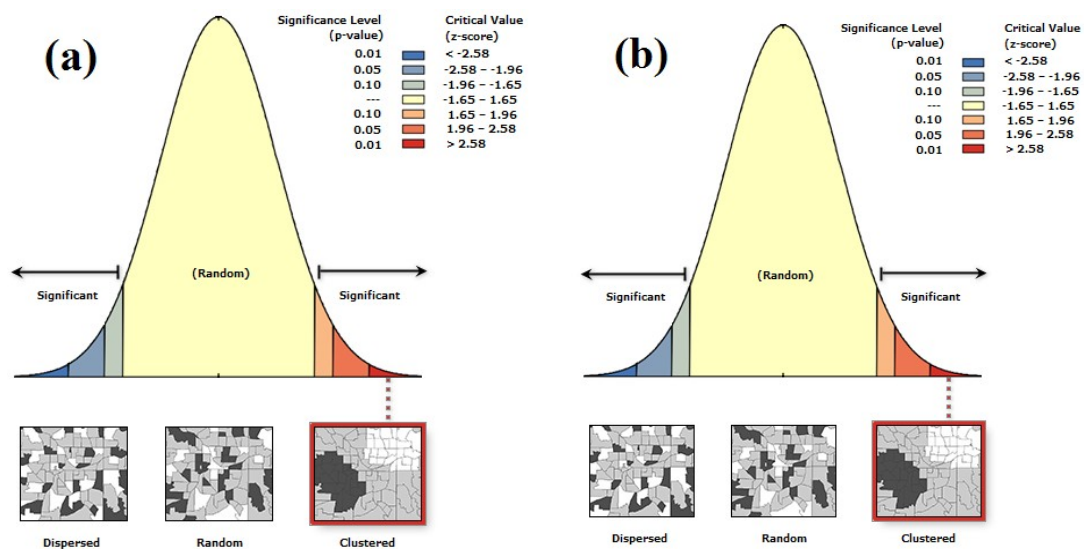

Figure 8. Result of Moran's I index for (**a**) the forest fire years and (**b**) the FRP.

Table 3. Result of Moran's I index parameters.

Moran's I Parameter	Year	FRP
Moran's Index	0.830061	0.904367
Variance	0.000248	0.000248
z-score	52.908683	57.726046
p-value	0	0

The results for the forest fire hotspots are shown in Figure 9. The results of both the year and the FRP parameters showed that the northwestern part of the study area had hot spots and the rest of the regions had cold and accidental spots.
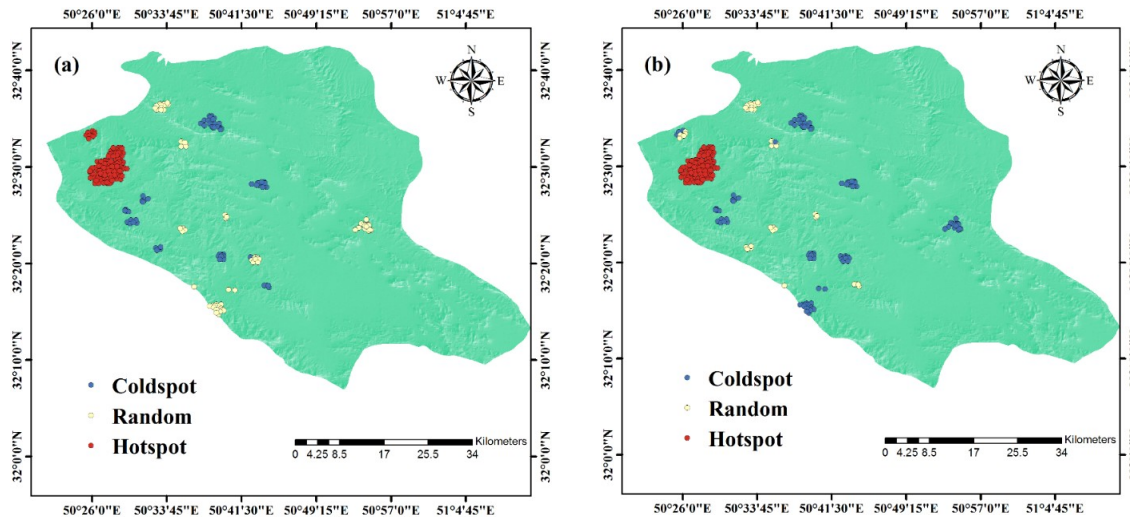

Figure 9. Forest fire hotspot analysis of (**a**) the forest fire years and (**b**) the FRP.

4.3. Results of FR

Table 4 presents the outcomes of the spatial relationship between the efficient factors and a fire location. The result of the altitude factor revealed that the highest FR (2.81) was associated with the altitude class greater than 2600 m. For the slope factor, the maximum FR value (1.67) was associated with the category of 15°–20°. According to the result of the slope aspect, it was found that the highest FR (1.23) pertained to the southwest direction. In the distance to a road factor, the 300–600 m class was found to have the highest FR (1.42). In the distance to a settlement factor, the highest FR (2.096) was related to the 0–500 m class. The Entisol group had the highest FR (1.39) in the soil type factor. The highest FR (5.96) in the rainfall factor was associated with the 750 mm class. In the temperature class, the class of 8 °C had the highest FR (4.06). In the wind effect factor, the highest FR (2.21) was related to the class greater than 1.2. The highest FR (1.8) in the land use/cover factor was associated with the forest class.

Table 4. Result of the FR model.

Class		No. of Pixels in Domain	No. of Fires	FR	Class		No. of Pixels in Domain	No. of Fires	FR
Altitud	<2000	43,836	0	0	**Land Use/Cover**	Forest	239,286	69	1.8
	2000–2200	380,953	9	0.14		Agriculture	285,290	33	0.72
	2200–2400	402,336	35	0.54		Pasture	589,141	81	0.86
	2400–2600	208,605	88	2.64		Urban	23,535	0	0
	>2600	113,617	51	2.81		Bare land	11,785	0	0
Slope Angle	0–5	476,815	34	0.48	**Distance to Settlements**	0–500	8989	3	2.096
	5–10	269,176	52	1.21		500–1000	25,606	3	0.73
	10–15	158,124	40	1.58		1000–1500	40,986	3	0.45
	15–20	100,963	27	1.67		1500–2000	56,353	11	1.22
	>20	134,369	30	1.4		>2000	101,741	163	1.006
Distance to Roads	0–300	84,252	18	1.34	**Rainfall**	<450	741,900	30	0.25
	300–600	70,352	16	1.42		450–550	162,761	29	1.11
	600–900	68,477	13	1.19		550–650	107,151	17	0.99
	900–1200	62,709	11	1.1		650–750	65,937	39	3.71
	>1200	633,557	125	0.9		>750	71,598	68	5.96

Table 4. *Cont.*

Class		No. of Pixels in Domain	No. of Fires	FR	Class		No. of Pixels in Domain	No. of Fires	FR
Temperature	< 8	138,900	90	4.06	Wind Effect	< 0.85	109,978	6	0.34
	7–9	217,489	53	1.53		0.85–1	489,524	28	0.35
	9–10	312,511	28	0.562		1–1.2	428,056	106	1.55
	10–11	210,520	0	0		>1.2	121,789	43	2.21
	>11	269,927	12	0.279					
Slope Aspect	Flat	11,412	1	0.55	Soil	Entisols	727,652	162	1.39
	N	161,213	21	0.81					
	NE	159,845	22	0.86		Inceptisols	319,998	21	0.41
	E	166,211	26	0.98					
	SE	106,608	21	1.23					
	S	162,467	28	1.08					
	SW	141,008	25	1.11		Rock Outcrops	101,392	01149042	0
	W	147,469	30	1.27					
	NW	93,114	9	0.6					

4.4. Results of the ANFIS-GA-SA Model

In order to implement the hybrid model and create the training and test datasets, 70% of the past fire locations (183 locations) with values of 1 and 183 locations were randomly assigned to the study area with zero values and 30% of the past fire locations (79 locations) with values of 1 and 79 locations were also randomly assigned to the study area with a value of zero being used. Preparing the data for a hybrid model was performed using an ArcGIS 10.3 software. The Matlab 2017b software was used to implement the hybrid model. Table 5 displays the parameters used by the hybrid algorithm.

Table 5. Parameters used in GA-SA algorithm.

Parameters	Value
Population	100
Iteration	1000
Interior iteration	10
Prime temperature	10
Crossover rate	0.7
Mutation rate	0.5

The results of the RMSE, MSE and MAE parameters in the hybrid algorithm for the training data were 0.2672, 0.0713 and 0.1735, respectively. The results of the RMSE, MSE and MAE parameters in the hybrid algorithm for the test data were 0.4286, 0.1837 and 0.2963, respectively. The convergence diagram for the objective function in the hybrid algorithm is shown in Figure 10. Figure 11 shows the performance of the hybrid algorithm for the training and the testing data. The trained network was applied to all pixels in the study area after training the model with the hybrid algorithm, and the FFSM was prepared in ArcGIS 10.3 software. The FFSM was subsequently split into five very low, low, medium, high and very high risk classifications (Figure 12).
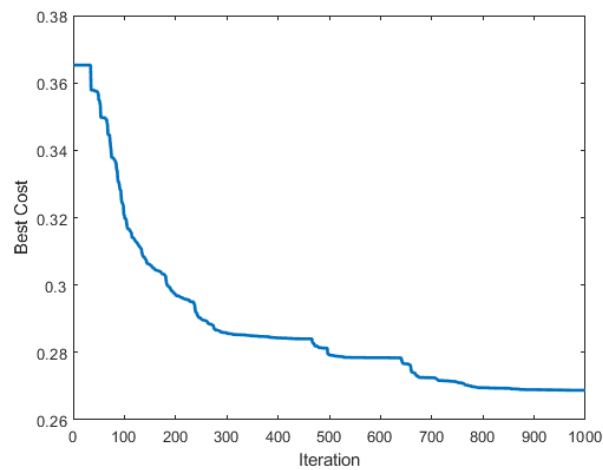
Figure 10. Objective function convergence diagram (GA-SA algorithm).
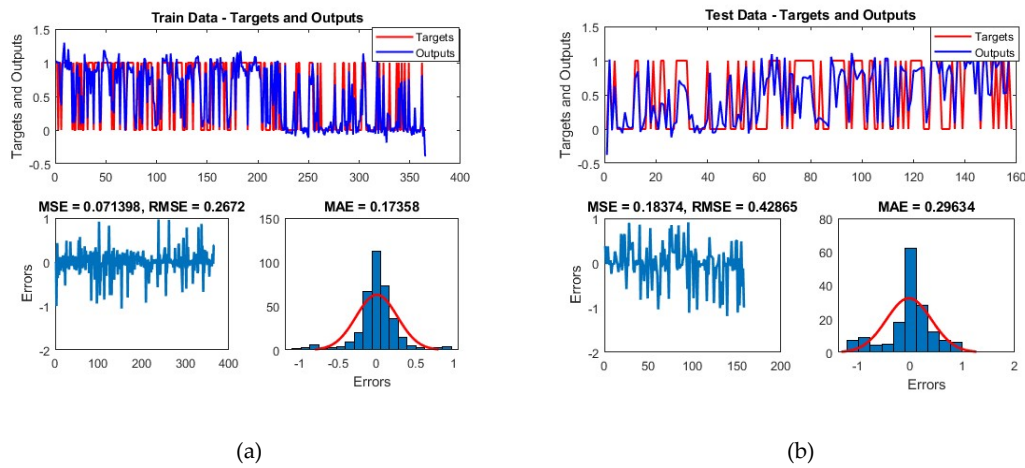

(a)　　　　　　　　　　　　　　　　　　　　　　　　(b)

Figure 11. Result of the ANFIS-GA-SA model with the (**a**) training data and (**b**) testing data.
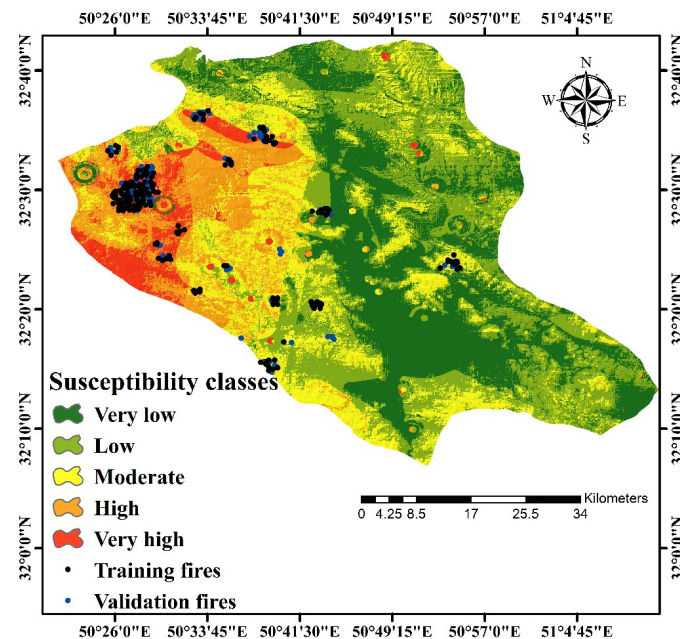

Figure 12. Fire susceptibility mapping (FFSM) using the ANFIS-GA-SA model.

4.5. Results of RBF-ICA Model

　　To implement the RBF-ICA model, the conditioning factors were divided into continuous and discrete categories. For each class of continuous factors, the weights obtained by the FR model were used. The training data were then chosen for the centers of each class to estimate the best fitting value. In Figure 13, the best fit for each factor was shown using the ensemble model. Based on Figure 13, the horizontal axis is the value of each factor, and the vertical axis is the value of the FR. In order to implement the ensemble model, the Matlab 2017b software was used. The parameters used in the colonial competition algorithm are shown in Table 6. The values of the continuous factors were transmitted to the ArcGIS 10.3 software and combined with the weight maps for the discrete factors obtained from the FR model. The final FFSM was prepared in five classes using the classification natural break method (Figure 14).
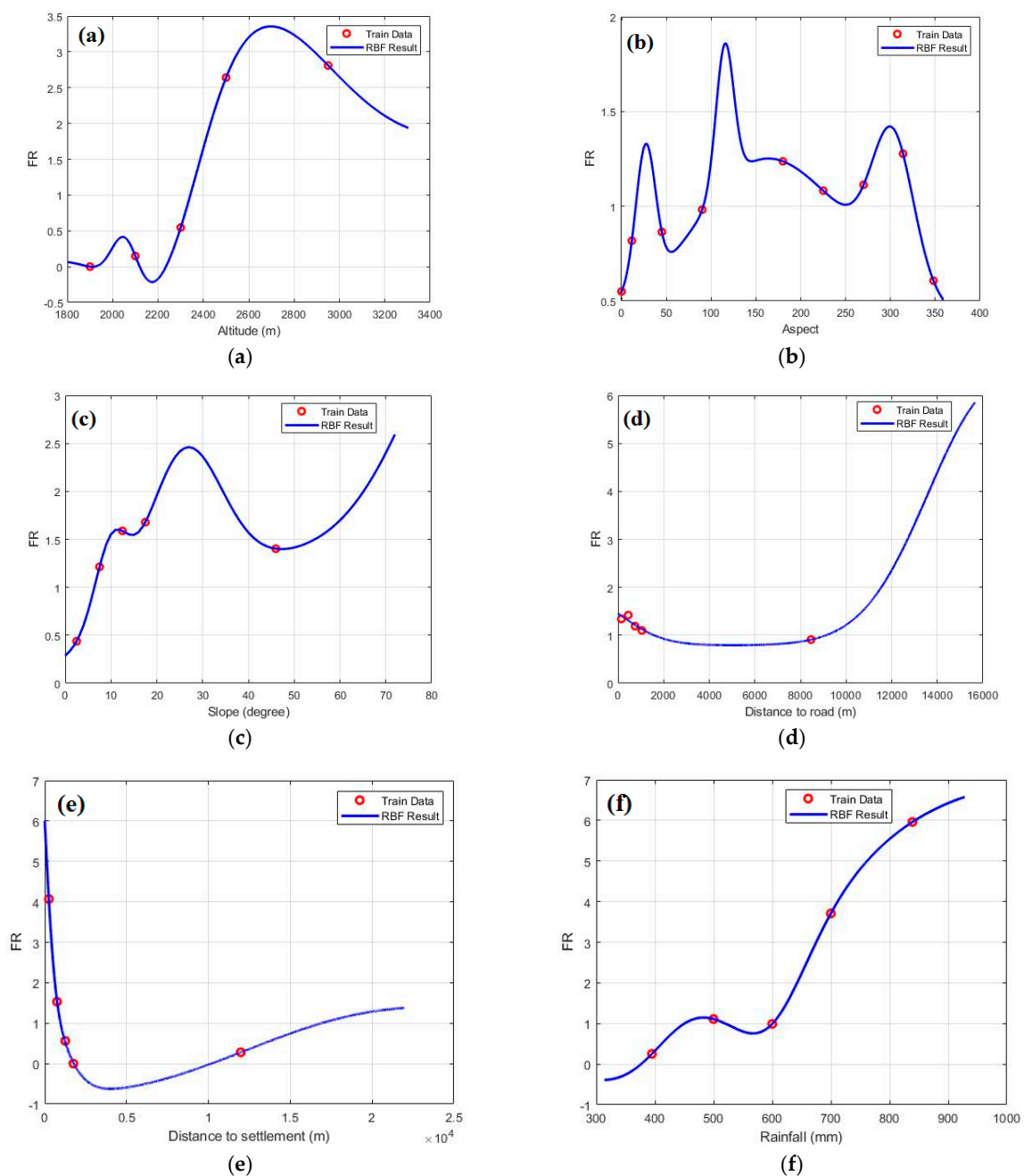

(a)

(b)

(c)

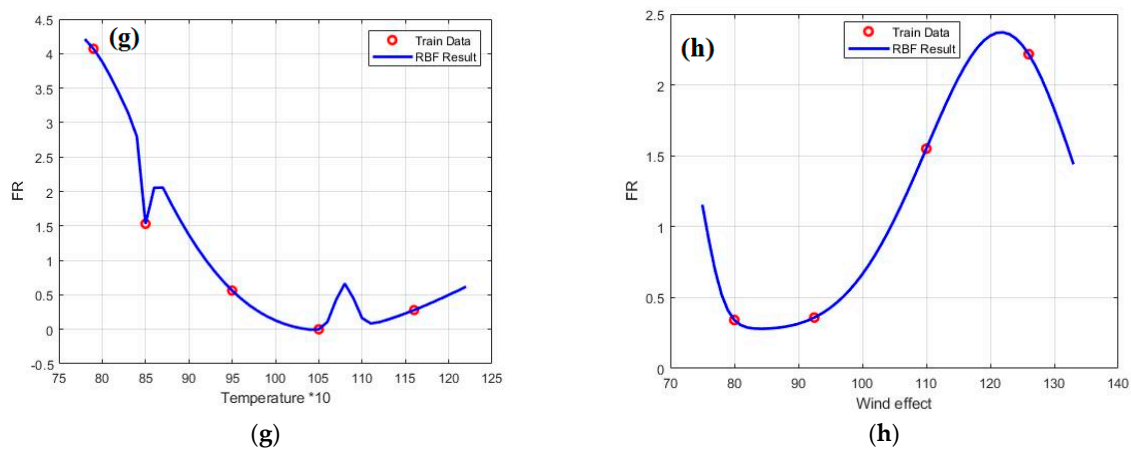(d)

(e)

(f)

Figure 13. *Cont.*

Figure 13. Result of the RBF-ICA model: (**a**) Altitude (**b**) Aspect (**c**) Slope (**d**) Distance to road (**e**) Distance to settlement (**f**) Rainfall (**g**) Temperature (**h**) Wind effect.

Table 6. Parameters used in the ICA algorithm.

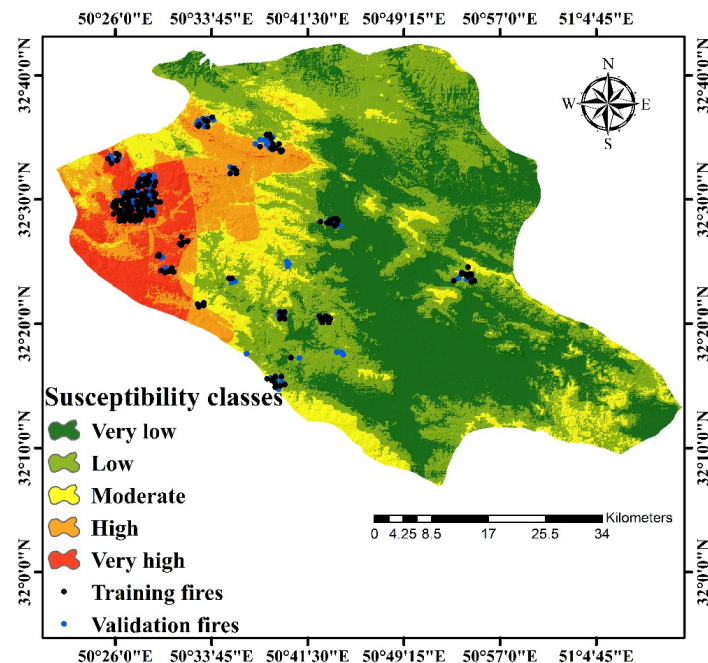| Parameters	Value
Population	40
Iteration	1000
Number of empires	10
Colonies mean cost coefficient	0.1
Selection pressure	1
Revolution probability	0.1
Revolution rate	0.5
Assimilation coefficient	2

Figure 14. FFSM using the RBF-ICA model.

4.6. Results of a Ubiquitous GIS-Based FFSM

After providing the FFSMs using the RBF-ICA and the ANFIS-SA-GA models, to provide users with easy access to maps produced at any time and at any location using ubiquitous GIS capabilities, the final forest fire maps were provided using the Open Layers library on the web GIS (http://uffsm.ir/).

In order to provide comprehensive results in a ubiquitous environment, an application was developed and implemented for a mobile platform in an android studio environment. In addition to displaying online FFSMs, the program features other capabilities, such as displaying the weather condition, temperature, pressure and the humidity in different areas and the GPS positioning. The designed interface is shown in Figure 15.
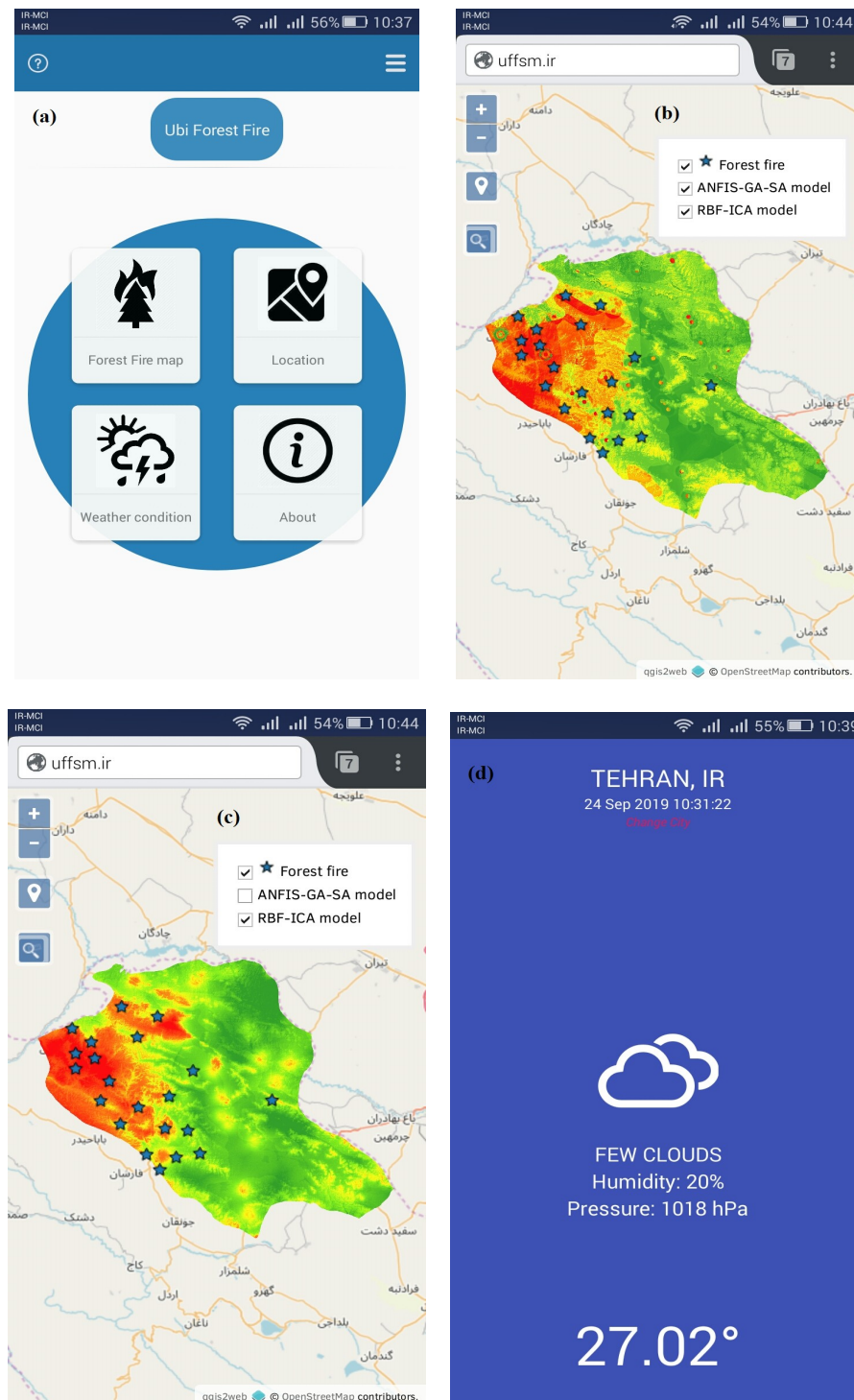

Figure 15. Mobile application developed: (**a**) Main menu (**b**) Result of ANFIS-GA-SA (**c**) Result of RBF-ICA (**d**) Weather condition.

4.7. Results Validation

To evaluate the final FFSM with the ROC curves, 79 fire positions (1 value) and 79 random points (0 value) were used. Figure 16 and Table 7 show the results for the ROC-AUC. Based on the results, the ANFIS-GA-SA and the RBF-ICA models have an accuracy of 0.903 and 0.878, respectively. Table 8 shows the results for the ANFIS-GA-SA model's RMSE and MAE parameters. Based on the results, the RMSE and the MAE parameter values for the training data and test data were 0.267, 0.173, 0.428 and 0.296, respectively.
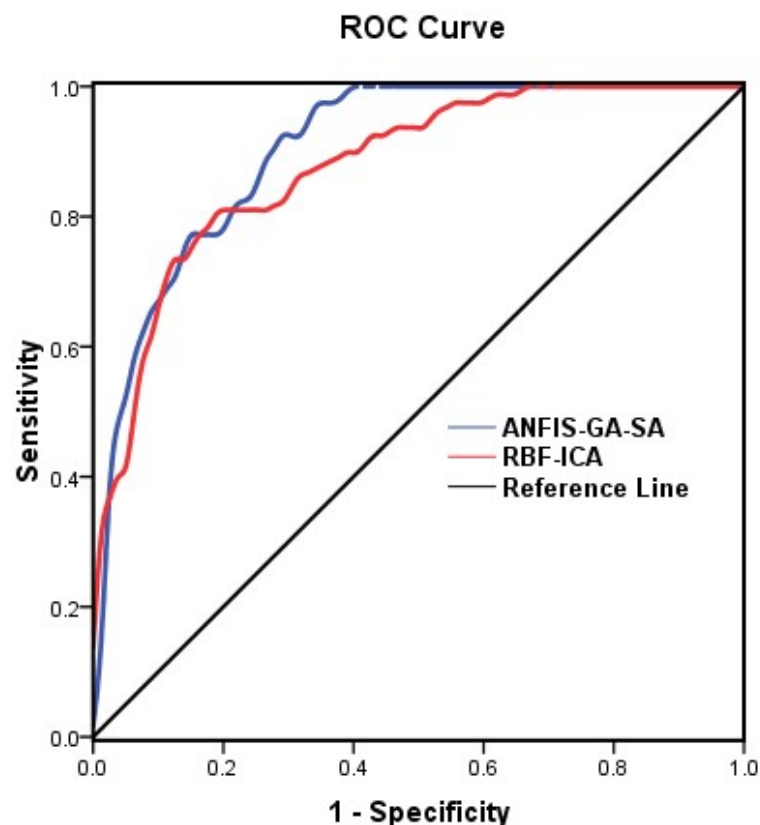

Figure 16. Result of the ROC curve.

Table 7. Result of the area under the curve (AUC) for the two models.

Test Result Variable(s)	Area	Std. Error	Asymptotic Sig	Asymptotic 95% Confidence Interval	
				Lower Bound	Upper Bound
ANFIS-GA-SA	0.903	0.024	0.000	0.856	0.949
RBF-ICA	0.878	0.027	0.000	0.826	0.930

Table 8. Result of the validation parameters.

ANFIS-GA-SA	Train	Test
Root mean square error (RMSE)	0.267	0.428
Mean absolute error (MAE)	0.173	0.296

5. Discussion

The results of the fire frequency and the fire cycle showed that the highest number of fires occurred in 2018 and 2016, respectively. According to the results, the FRP data have less spatial autocorrelation than the fire year, and on the other hand, fire year data have more spatial variance than the FRP. The value of the SD index for the year and the FRP parameters is less than 25%, which indicates the

strong spatial dependence of these two parameters. Moreover, the parameter of the year had a stronger spatial dependence, more spatial stability and fewer observation errors than the FRP parameter. Among the variables affecting forest fires, the distance to settlements, soil and the rainfall variables have the highest spatial dependence and the slope angle, slope aspect the and wind effect variables have the least spatial dependence. Based on the results of the range parameter, the temperature, land use/cover and the distance to road variables have the least spatial variability and the soil, slope angle and the slope aspect variables have the most spatial variability. The results of the spatial autocorrelation showed that the hot spots of fire have a cluster distribution and the hot areas of the fire correspond to the maps prepared with ANFIS-GA-SA and RBF-ICA models.

Based on the spatial relationship between the efficient factors and a fire location by the FR model, it was concluded that in the altitude factor, the maximum FR value was for the category of more than 2600 m. This is because of the proximity of the forests to the mountainous regions in the studied areas. In the slope angle factor, the highest weight belonged to the class of 15–20 degrees, which may be due to the higher density of vegetation in this class and also the likelihood of fires in sloped areas [18]. In the slope aspect factor, the highest weight is associated with the west and southeast classes. Southern directions have more light, temperature and wind with less humidity and fuels. The vegetation in the southern aspect is drier and less dense than in the northern aspect, and it is more prone to combustion [50]. In the distance to a road factor, it showed that as the distance to a road increases, the fires are reduced. Near the roads, humans have more access to the forest and can cause forest fires. This is consistent with the result presented by Jaafari et al. [14]. The distance to a settlement factor indicates that the occurrence of fires is reduced when the distance to a settlement increases, which is consistent with that of Jaafari et al. [2]. Other findings showed that in the land use/cover factor, the class of forest is more prone to fires than pastures and agricultural classes. The analysis of the temperature and rainfall variables indicated that the risk of fires in the study area was associated a with lower temperature and more rainfall. From the results of these two climatic parameters, it can be concluded that fires occur more frequently in elevated mountainous areas. As the wind effect increases, the likelihood of fires increases, which is consistent with Pourtaghi et al. [18]. In the soil factor, it was concluded that the Entisols class was associated with more fire occurrences, which is due to the fact that 63% of the study area was covered with Entisols. Overall, it can be concluded that most of the fires occurred in elevated areas, and the topography played a major role in the occurrence of the fires in the study area.

In fuzzy systems, the number of rules for modeling in the network structure will be greater with the increasing membership functions in the input space. Since each membership function has its own adjustable parameter, this caused the pre-fitness problem. Therefore, it is important to use specific methods to optimize the number of rules and parameters. In order to optimize the ANFIS model, the GA-SA algorithm was used. However, each of the metaheuristic algorithms has advantages and disadvantages. Combining these algorithms was a method to increase their accuracy and eliminate their disadvantages. One of the advantages of the GA algorithm is being population-based, and it uses a crossover and mutation operator to select the best offspring. The low convergence rate and limited local search for optimal results are some of disadvantages of the GA algorithm. On the other hand, a high convergence and a wider local search in the SA algorithm eliminates the disadvantages of the GA algorithm. In addition, the SA algorithm increases the accuracy of optimization by using the initial population of the GA algorithm as well as the crossover and mutation parameters.

In natural hazards, since conditioning factors are not in a crisp state, the model cannot be suitable for modeling natural hazards. For example, the class with less than 2200 m has an FR value of 0 in the altitude parameter. This value is assigned to the altitude between 0–2200 m. However, the altitude of 600 m may have a different weight from 2200 m. To overcome this problem, we used the RBF interpolation method to obtain a specific weight for each value. The RBF interpolation method features multivariate distributed data. We used the ICA to adjust the RBF coefficients. One of the advantages of the ICA algorithm is the novelty of the basic idea of the algorithm, its ability to optimize equilibrium

even in the face of various optimization problems compared to other optimization algorithms and its speed to find the optimal answer [70].

According to the ROC-AUC results, the ANFIS-GA-SA model was more accurate than the RBF-ICA model with preparing the FFSM. The reason for this is that it uses a fuzzy inference system (FIS) in the ANFIS model, which requires linguistic rules as its basic information for modeling. In addition, the input and output variables in this model were described linguistically. Therefore, if the information is incomplete and inconsistent, the fuzzy system must adapt itself to these conditions.

Preparing the FFSM in the ubiquitous system in the form of GIS and mobile GIS applications makes it easier for users to access these maps at any time and place. It also provides the users with more comprehensive information about the underlying maps. The ubiquitous system receives more information than two-dimensional maps.

6. Conclusions

The purpose of this study was to prepare the FFSM using ubiquitous GIS and ANFIS-GA-SA and RBF-ICA models in the Chaharmahal and Bakhtiari Province, Iran. The research results were as follows:

1. Based on ROC-AUC analysis, the ANFIS-GA-SA model was more effective in preparing the FFSM than the RBF-ICA model.

2. Combining the metaheuristic algorithms to optimize the ANFIS eliminated the deficiency of each algorithm.

3. Using a ubiquitous GIS system made it possible to display a hazard map and allow users to interact more effectively with the hazard maps.

4. Based on the FR model results, the fire in the study area occurrence was higher in an altitude of more than 2600 m, a slope angle between 15–20°, a west slope aspect, a distance to a settlement less than 500 m, a distance to a road between 300 and 600 m, rainfall between more than 750 mm, temperature less than 8 °C, a wind effect more than 1.2, forest in land use/cover and Entisols soil.

Author Contributions: Data curation, S.V.R.-T.; Formal analysis, S.V.R.-T. and A.S.-N.; Funding acquisition, S.-M.C.; Methodology, S.V.R.-T and A.S.-N.; Project administration, S.-M.C.; Resources, A.S.-N.; Software, S.V.R.-T.; Supervision, A.S.-N.; Validation, S.-M.C. and A.S.-N.; Writing—original draft, S.V.R.-T.; Writing —review and editing, A.S.-N. and S.-M.C. All authors have read and agreed to the published version of the manuscript.

Conflicts of Interest: The authors declare no conflict of interest.

References

1. Wali, M.K.; Watts, S.E. Forest ecology. *J. Environ. Qual.* **1999**, *28*, 1683–1685. [CrossRef]
2. Jaafari, A.; Termeh, S.V.R.; Bui, D.T. Genetic and firefly metaheuristic algorithms for an optimized neuro-fuzzy prediction modeling of wildfire probability. *J. Environ. Manag.* **2019**, *243*, 358–369. [CrossRef] [PubMed]
3. Yin, H.-W.; Kong, F.-H.; Li, X.-Z. Rs and gis-based forest fire risk zone mapping in da hinggan mountains. *Chin. Geogr. Sci.* **2004**, *14*, 251–257. [CrossRef]
4. Ketterings, Q.M.; Wibowo, T.T.; van Noordwijk, M.; Penot, E. Farmers' perspectives on slash-and-burn as a land clearing method for small-scale rubber producers in sepunggur, jambi province, sumatra, indonesia. *For. Ecol. Manag.* **1999**, *120*, 157–169. [CrossRef]
5. Adab, H.; Kanniah, K.D.; Solaimani, K. Modeling forest fire risk in the northeast of iran using remote sensing and gis techniques. *Nat. Hazards* **2013**, *65*, 1723–1743. [CrossRef]
6. Sarkargar Ardakani, A.; Valdan Zouj, M.; Mansoorian, A. Spatial analysis of fire potential in iran different region by using rs and gis. *J. Environ. Sci.* **2009**, *35*, 25–34.
7. Jaafari, A.; Pourghasemi, H.R. Factors influencing regional-scale wildfire probability in iran: An application of random forest and support vector machine. In *Spatial Modeling in GIS and R for Earth and Environmental Sciences*; Elsevier: Amsterdam, The Netherlands, 2019; pp. 607–619.

8.   Adab, H.; Kanniah, K.D.; Solaimani, K.; Sallehuddin, R. Modelling static fire hazard in a semi-arid region using frequency analysis. *Int. J. Wildland Fire* **2015**, *24*, 763–777. [CrossRef]

9.   Pradhan, B.; Suliman, M.D.H.B.; Awang, M.A.B. Forest fire susceptibility and risk mapping using remote sensing and geographical information systems (gis). *Disaster Prev. Manag. Int. J.* **2007**, *16*. [CrossRef]

10.   Pourghasemi, H.R. Gis-based forest fire susceptibility mapping in iran: A comparison between evidential belief function and binary logistic regression models. *Scand. J. For. Res.* **2016**, *31*, 80–98. [CrossRef]

11.   Karimi, A.; Abdollahi, S.; Ostad-Ali-Askari, K.; Singh, V.P.; Eslamian, S.; Heidarian, A.; Nekooei, M.; Gholami, H.; Pazdar, S. Evaluating models and effective factors obtained from remote sensing (rs) and geographic information system (gis) in the prediction of forest fire risk, structured review. *J. Geogr. Cartogr.* **2018**, *1*. [CrossRef]

12.   Hong, H.; Naghibi, S.A.; Dashtpagerdi, M.M.; Pourghasemi, H.R.; Chen, W. A comparative assessment between linear and quadratic discriminant analyses (lda-qda) with frequency ratio and weights-of-evidence models for forest fire susceptibility mapping in china. *Arab. J. Geosci.* **2017**, *10*, 167. [CrossRef]

13.   Nami, M.; Jaafari, A.; Fallah, M.; Nabiuni, S. Spatial prediction of wildfire probability in the hyrcanian ecoregion using evidential belief function model and gis. *Int. J. Environ. Sci. Technol.* **2018**, *15*, 373–384. [CrossRef]

14.   Jaafari, A.; Gholami, D.M.; Zenner, E.K. A bayesian modeling of wildfire probability in the zagros mountains, iran. *Ecol. Inform.* **2017**, *39*, 32–44. [CrossRef]

15.   Gigović, L.; Pourghasemi, H.R.; Drobnjak, S.; Bai, S. Testing a new ensemble model based on svm and random forest in forest fire susceptibility assessment and its mapping in serbia's tara national park. *Forests* **2019**, *10*, 408. [CrossRef]

16.   Sachdeva, S.; Bhatia, T.; Verma, A. Gis-based evolutionary optimized gradient boosted decision trees for forest fire susceptibility mapping. *Natural Hazards* **2018**, *92*, 1399–1418. [CrossRef]

17.   Bui, D.T.; Bui, Q.-T.; Nguyen, Q.-P.; Pradhan, B.; Nampak, H.; Trinh, P.T. A hybrid artificial intelligence approach using gis-based neural-fuzzy inference system and particle swarm optimization for forest fire susceptibility modeling at a tropical area. *Agric. For. Meteorol.* **2017**, *233*, 32–44.

18.   Pourtaghi, Z.S.; Pourghasemi, H.R.; Aretano, R.; Semeraro, T. Investigation of general indicators influencing on forest fire and its susceptibility modeling using different data mining techniques. *Ecol. Indic.* **2016**, *64*, 72–84. [CrossRef]

19.   Dimuccio, L.A.; Ferreira, R.; Cunha, L.; de Almeida, A.C. Regional forest-fire susceptibility analysis in central portugal using a probabilistic ratings procedure and artificial neural network weights assignment. *Int. J. Wildland Fire* **2011**, *20*, 776–791. [CrossRef]

20.   Suryabhagavan, K.; Alemu, M.; Balakrishnan, M. Gis-based multi-criteria decision analysis for forest fire susceptibility mapping: A case study in harenna forest, southwestern ethiopia. *Trop. Ecol.* **2016**, *57*, 33–43.

21.   Lv, Z.; Réhman, S.U.; Chen, G. Webvrgis: A p2p Network Engine for VR Data and GIS Analysis. In Proceedings of the International Conference on Neural Information Processing, Daegu, Germany, 3–7 November 2013; Springer: Berlin/Heidelberg, Germany; pp. 503–510.

22.   Debevec, P.E.; Taylor, C.J.; Malik, J. Modeling and rendering architecture from photographs: A hybrid geometry-and image-based approach. In Proceedings of the 23rd Annual Conference on Computer Graphics and Interactive Techniques, New Orleans, LA, USA, 4–9 August 1996; pp. 11–20.

23.   Kim, S.K.; Lee, J.H.; Ryu, K.H.; Kim, U. A framework of spatial co-location pattern mining for ubiquitous gis. *Multimed. Tools Appl.* **2014**, *71*, 199–218. [CrossRef]

24.   Jaafari, A.; Zenner, E.K.; Panahi, M.; Shahabi, H. Hybrid artificial intelligence models based on a neuro-fuzzy system and metaheuristic optimization algorithms for spatial prediction of wildfire probability. *Agric. For. Meteorol.* **2019**, *266*, 198–207. [CrossRef]

25.   Dong, C.; Liu, F.; Wang, H.; Chen, F. Application Research of Mobile GIS in Forestry Informatization. In Proceedings of the 5th International Conference on Computer Science & Education, Hefei, China, NJ, USA, 24–27 August 2010; IEEE: Piscataway, NJ, USA; pp. 351–355.

26.   Battad, D.; Mackenzie, P. Applications of mobile gis in forestry south australia. *Int. Arch. Photogramm. Remote Sens. Spat. Inf. Sci.* **2012**, *39*, 447–452. [CrossRef]

27.   Kalabokidis, K.; Athanasis, N.; Gagliardi, F.; Karayiannis, F.; Palaiologou, P.; Parastatidis, S.; Vasilakos, C. Virtual fire: A web-based gis platform for forest fire control. *Ecol. Inform.* **2013**, *16*, 62–69. [CrossRef]

28. Roberto Barbosa, M.; Carlos Sicoli Seoane, J.; Guimaraes Buratto, M.; Santana de Oliveira Dias, L.; Paulo Carvalho Raivel, J.; Lobos Martins, F. Forest fire alert system: A geo web gis prioritization model considering land susceptibility and hotspots—A case study in the carajás national forest, brazilian amazon. *Int. J. Geogr. Inf. Sci.* **2010**, *24*, 873–901. [CrossRef]

29. Jeefoo, P. Wildfire field survey using mobile GIS technology in Nan province. In Proceedings of the 2019 Joint International Conference on Digital Arts, Media and Technology with ECTI Northern Section Conference on Electrical, Electronics, Computer and Telecommunications Engineering (ECTI DAMT-NCON), Nan, Thailand, 30 January–2 February 2019; IEEE: Piscataway, NJ, USA, 2019; pp. 98–100.

30. Moayedi, H.; Mehrabi, M.; Bui, D.T.; Pradhan, B.; Foong, L.K. Fuzzy-metaheuristic ensembles for spatial assessment of forest fire susceptibility. *J. Environ. Manag.* **2020**, *260*, 109867. [CrossRef] [PubMed]

31. Hong, H.; Tsangaratos, P.; Ilia, I.; Liu, J.; Zhu, A.-X.; Xu, C. Applying genetic algorithms to set the optimal combination of forest fire related variables and model forest fire susceptibility based on data mining models. The case of dayu county, china. *Sci. Total Environ.* **2018**, *630*, 1044–1056. [CrossRef]

32. Zhang, G.; Wang, M.; Liu, K. Forest fire susceptibility modeling using a convolutional neural network for yunnan province of china. *Int. J. Disaster Risk Sci.* **2019**, *10*, 386–403. [CrossRef]

33. Bui, Q.-T. Metaheuristic algorithms in optimizing neural network: A comparative study for forest fire susceptibility mapping in dak nong, vietnam. *Geomat. Nat. Hazards Risk* **2019**, *10*, 136–150. [CrossRef]

34. Jaafari, A.; Najafi, A.; Pourghasemi, H.; Rezaeian, J.; Sattarian, A. Gis-based frequency ratio and index of entropy models for landslide susceptibility assessment in the caspian forest, northern iran. *Int. J. Environ. Sci. Technol.* **2014**, *11*, 909–926. [CrossRef]

35. Jang, J.-S. Anfis: Adaptive-network-based fuzzy inference system. *IEEE Trans. Syst. Manand Cybern.* **1993**, *23*, 665–685. [CrossRef]

36. Yaghoobi, A.; Bakhshi-Jooybari, M.; Gorji, A.; Baseri, H. Application of adaptive neuro fuzzy inference system and genetic algorithm for pressure path optimization in sheet hydroforming process. *Int. J. Adv. Manuf. Technol.* **2016**, *86*, 2667–2677. [CrossRef]

37. Sivanandam, S.; Deepa, S. Genetic algorithms. In *Introduction to Genetic Algorithms*; Springer: Berlin/Heidelberg, Germany, 2008; pp. 15–37.

38. Mukhopadhyay, D.M.; Balitanas, M.O.; Farkhod, A.; Jeon, S.-H.; Bhattacharyya, D. Genetic algorithm: A tutorial review. *Int. J. Grid Distrib. Comput.* **2009**, *2*, 25–32.

39. Ravagnani, M.; Silva, A.; Arroyo, P.; Constantino, A. Heat exchanger network synthesis and optimisation using genetic algorithm. *Appl. Therm. Eng.* **2005**, *25*, 1003–1017. [CrossRef]

40. Kirkpatrick, S.; Gelatt, C.D.; Vecchi, M.P. Optimization by simulated annealing. *Science* **1983**, *220*, 671–680. [CrossRef]

41. Misevičius, A. A modified simulated annealing algorithm for the quadratic assignment problem. *Informatica* **2003**, *14*, 497–514. [CrossRef]

42. Dudek, G. Adaptive simulated annealing schedule to the unit commitment problem. *Electr. Power Syst. Res.* **2010**, *80*, 465–472. [CrossRef]

43. Atashpaz-Gargari, E.; Lucas, C. Imperialist competitive algorithm: An algorithm for optimization inspired by imperialistic competition. In Proceedings of the IEEE Congress on Evolutionary Computation, Singapore, 25–28 September 2007; IEEE: Piscataway, NJ, USA; pp. 4661–4667.

44. Talatahari, S.; Azar, B.F.; Sheikholeslami, R.; Gandomi, A. Imperialist competitive algorithm combined with chaos for global optimization. *Commun. Nonlinear Sci. Numer. Simul.* **2012**, *17*, 1312–1319. [CrossRef]

45. Schueremans, L.; Van Gemert, D. Benefit of splines and neural networks in simulation based structural reliability analysis. *Struct. Saf.* **2005**, *27*, 246–261. [CrossRef]

46. Jaiswal, R.K.; Mukherjee, S.; Raju, K.D.; Saxena, R. Forest fire risk zone mapping from satellite imagery and gis. *Int. J. Appl. Earth Obs. Geoinf.* **2002**, *4*, 1–10. [CrossRef]

47. Chuvieco, E.; Congalton, R.G. Application of remote sensing and geographic information systems to forest fire hazard mapping. *Remote Sens. Environ.* **1989**, *29*, 147–159. [CrossRef]

48. Vadrevu, K.P.; Eaturu, A.; Badarinath, K. Fire risk evaluation using multicriteria analysis—A case study. *Environ. Monit. Assess.* **2010**, *166*, 223–239. [CrossRef] [PubMed]

49. Chandra, S. Application of remote sensing and gis technology in forest fire risk modeling and management of forest fires: A case study in the garhwal himalayan region. In *Geo-Information for Disaster Management*; Springer: Berlin/Heidelberg, Germany, 2005; pp. 1239–1254.

50. Eskandari, S.; Chuvieco, E. Fire danger assessment in iran based on geospatial information. *Int. J. Appl. Earth Obs. Geoinf.* **2015**, *42*, 57–64. [CrossRef]

51. Perera, A.H.; Euler, D.L.; Thompson, I.D. *Ecology of a Managed Terrestrial Landscape: Patterns and Processes of Forest Landscapes in Ontario*; UBC Press: Vancouver, BC, USA, 2011.

52. Lim, C.-H.; Kim, Y.S.; Won, M.; Kim, S.J.; Lee, W.-K. Can satellite-based data substitute for surveyed data to predict the spatial probability of forest fire? A geostatistical approach to forest fire in the republic of korea. *Geomat. Nat. Hazards Risk* **2019**, *10*, 719–739. [CrossRef]

53. Webster, R.; Oliver, M.A. *Geostatistics for Environmental Scientists*; John Wiley & Sons: Hoboken, NJ, USA, 2007.

54. Gunnarsson, F.; Holm, S.; Holmgren, P.; Thuresson, T. On the potential of kriging for forest management planning. *Scand. J. For. Res.* **1998**, *13*, 237–245. [CrossRef]

55. Ziegel, E.R. Geostatistics for environmental scientists. *Technometrics* **2001**, *43*, 499.

56. Anselin, L. Local indicators of spatial association—Lisa. *Geogr. Anal.* **1995**, *27*, 93–115. [CrossRef]

57. Getis, A.; Ord, J. The analysis of spatial association by use of distance statistics, geographycal analysis. In *Perspectives on Spatial Data Analysis*; Springer: Berlin/Heidelberg, Germany, 1992.

58. Odland, J. *Spatial Autocorrelation*; SAGE Publications, Incorporated: New York, NY, USA, 1988; Volume 9.

59. Haznedar, B.; Kalinli, A. Training anfis using genetic algorithm for dynamic systems identification. *Int. J. Intell. Syst. Appl. Eng.* **2016**, 44–47. [CrossRef]

60. Sarkheyli, A.; Zain, A.M.; Sharif, S. Robust optimization of anfis based on a new modified ga. *Neurocomputing* **2015**, *166*, 357–366. [CrossRef]

61. Yu, H.; Fang, H.; Yao, P.; Yuan, Y. A combined genetic algorithm/simulated annealing algorithm for large scale system energy integration. *Comput. Chem. Eng.* **2000**, *24*, 2023–2035. [CrossRef]

62. Termeh, S.V.R.; Kornejady, A.; Pourghasemi, H.R.; Keesstra, S. Flood susceptibility mapping using novel ensembles of adaptive neuro fuzzy inference system and metaheuristic algorithms. *Sci. Total Environ.* **2018**, *615*, 438–451. [CrossRef]

63. Aghdam, I.N.; Varzandeh, M.H.M.; Pradhan, B. Landslide susceptibility mapping using an ensemble statistical index (wi) and adaptive neuro-fuzzy inference system (anfis) model at alborz mountains (iran). *Environ. Earth Sci.* **2016**, *75*, 553. [CrossRef]

64. Weiser, M. The computer for the 21 st century. *Sci. Am.* **1991**, *265*, 94–105. [CrossRef]

65. Krumm, J. *Ubiquitous Computing Fundamentals*; Chapman and Hall/CRC: Boca Raton, FL, USA, 2016.

66. Truong, H.; Dustdar, S. Context coupling techniques. In *Enabling Context-Aware Web Services: Methods, Architectures, and Technologies*; Chapman and Hall/CRC: Boca Raton, FL, USA, 2010; pp. 337–364.

67. Li, K.-J. *Ubiquitous GIS, Part I: Basic Concepts of Ubiquitous GIS*; Lecture Slides, Pusan National University: Busan, Korea, 2007.

68. Razavi Termeh, V.; Sadeghi Niaraki, A. Design and implementation of ubiquitous health system (u-health) using smart-watches sensors. *Int. Arch. Photogramm. Remote Sens. Spat. Inf. Sci.* **2015**, *40*, 607–612. [CrossRef]

69. Razavi-Termeh, S.V.; Sadeghi-Niaraki, A.; Choi, S.-M. Groundwater potential mapping using an integrated ensemble of three bivariate statistical models with random forest and logistic model tree models. *Water* **2019**, *11*, 1596. [CrossRef]

70. Razavi-Termeh, S.V.; Sadeghi-Niaraki, A.; Choi, S.-M. Gully erosion susceptibility mapping using artificial intelligence and statistical models. *Geomat. Nat. Hazards Risk* **2020**, *11*, 821–845. [CrossRef]